New measurement of the $K^+ \to \pi^+ \nu\bar{\nu}$ branching ratio

version 1

E949 collaboration

July 25, 2008

Abstract

Three candidates for the decay $K^+ \to \pi^+ \nu\bar{\nu}$ have been observed in the pion momentum region $140 < P < 199$ MeV/c upon an estimated background of $0.927 \pm 0.168^{+0.320}_{-0.237}$ events. Combining these observations with previously reported results yields a branching fraction of $\mathcal{B}(K^+ \to \pi^+ \nu\bar{\nu}) = (1.73^{+1.15}_{-1.05}) \times 10^{-10}$.

The rate of $K^+ \to \pi^+ \nu\bar{\nu}$ decays is amongst a handful of hadronic processes that can be accurately predicted in the standard model (SM) owing to knowledge of the transition matrix element from similar processes and minimal long-distance effects [1]. The small precisely predicted branching fraction, $\mathcal{B}(K^+ \to \pi^+ \nu\bar{\nu}) = (0.85 \pm 0.07) \times 10^{-10}$ [2], and the fact that this decay is a flavor changing neutral current process makes it a sensitive probe of non-SM effects [1]. Previous studies of this decay by experiment E787 at Brookhaven National Laboratory and its successor E949 have measured $\mathcal{B}(K^+ \to \pi^+ \nu\bar{\nu}) = (1.47^{+1.30}_{-0.89}) \times 10^{-10}$ based on the observation of three candidates upon a total background of 0.44 ± 0.05 events in the pion momentum

region $211 < P < 229$ MeV/c (pnn1) above the $K^+ \to \pi^+\pi^0$ ($K_{\pi 2}$) peak [3] and set a consistent limit of $< 22 \times 10^{-10}$ at 90% C.L. based on one candidate upon a total background of 1.22 ± 0.24 events in the momentum region $140 < P < 195$ MeV/c (pnn2) below the $K_{\pi 2}$ peak [6].

In this Letter we report the results of a search for $K^+ \to \pi^+\nu\bar{\nu}$ below the $K_{\pi 2}$ peak using 1.7×10^{12} stopped K^+ decays obtained with E949 as well as the final results on $\mathcal{B}(K^+ \to \pi^+\nu\bar{\nu})$ from all E787 and E949 data.

The E949 apparatus and analysis of the data in the pnn1 region has been described elsewhere [4]. In this Letter, we concentrate on the apparatus and analysis features most relevant for pnn2. Identification of $K^+ \to \pi^+\nu\bar{\nu}$ decays relies on detection of an incoming kaon and outgoing pion with no other detector activity. A 710 MeV/c K^+ beam, produced by 21.5 GeV proton interactions on a platinum target, passed through two electomagnetostatic separators during transport to the E949 scintillating fiber target (TG). Typically 1.6×10^6 K^+/s entered the E949 TG during a 2.2 s spill with a K^+/π^+ ratio of $\sim$3.

Incoming kaons were identified by a Cerenkov counter and two proportional wire chambers before being slowed by an 11.1 cm thick BeO degrader and an active degrader (AD), passing through a beam hodoscope and stopping in the TG. The AD comprised 39 2.2 mm thick copper disks interleaved with 40 layers of 2.2 mm plastic scintillator divided into 12 azimuthal segments. Scintillation light from each segment was transported via wavelength shifting fibers to a photomultiplier tube (PMT) that was read out by time-

to-digital convertors (TDCs), GaAs CCD digitizers (CCDs) sampling at 500 MHz and analog-to-digital convertors (ADCs). The AD was capable of providing measurements of the incoming beam particle and activity concident with K^+ decay in the TG. The TG consists of 413 5mm square and 3.1 m long scintillating fibers packed into a 12 cm diameter cylinder. Each 5 mm fiber was connected to a PMT and read out by ADCs, TDCs and CCDs in order to provide measurements of activity in the TG coincident with both the incoming kaon and the outgoing pion.

The momentum, trajectory and position of the outgoing π^+ were measured in a drift chamber [7]. The outgoing pion was slowed to a stop in a range stack (RS) of 19 layers of plastic scintillator with 24 segments in azimuth. PMTs on each end of the scintillator were read out by ADCs, TDCs and 500-MHz transient digitizers (TDs) and enabled measurment of the pion range (R) and kinetic energy (E) as well as the $\pi^+ \to \mu^+ \to e^+$ decay sequence.

The barrel veto (BV) calorimeters of 16.6 radiation lengths at normal incidence provided photon vetoing over 2/3 of 4π sr solid angle. Photon vetoing over the remaining 1/3 of 4π was provided by upstream and downstream end caps of undoped CsI (13.5 r.l.), upstream (4.6 r.l.) and downstream (9.2 r.l.) collar counters, a downstream microcollar ($\sim$ 15 r.l.), an upstream photon veto (3.1 r.l.) and a downstream photon veto (DPV, 7.3 r.l.). The latter detectors all utilized lead/scintillator technology. The AD (6.1 r.l.) and target ($\sim$7.3 r.l.) also provided additional photon veto capability [4].

Data were acquired with a multilevel trigger that required an entering kaon to stop in the target followed by an outgoing particle leaving the target at least 1.5 ns later that was subsequently identified as a pion via the $\pi^+ \to \mu^+$ signature in the RS TD read out and accompanied by no other activity. Additional pre-scaled triggers were used to accumulate $\mathrm{K}^+ \to \mu^+\nu(\gamma)$ ($\mathrm{K}_{\mu 2(\gamma)}$) and $K_{\pi 2}$ decays as well as beam pions scattering in the target for monitoring and calibration purposes.

This analysis exploited previous experience [4] [5] [6] as well as detector upgrades of the AD, BV and DPV to increase signal acceptance by 40% compared to [6] while maintaining a comparable background rate. In addition the improved knowledge of the background contributions allowed the signal region to be divided into 9 sub-regions ("cells") with relative acceptance-to-background levels differing by a factor of ~ 4 that could be exploited by a likelihood method [8] to determine $\mathcal{B}(\mathrm{K}^+ \to \pi^+\nu\bar{\nu})$.

We employed a "blind" analysis technique in which the signal region was not examined until all signal candidate selection criteria ("cuts") were established, the estimate of all backgrounds were completed and acceptance of all cells determined. At least two uncorrelated cuts with significant rejection were created for most backgrounds. Inversion of one of the pair of cuts could then be used to select a background-enriched data sample containing N events. Inversion of the complementary cut selected a data sample on which the rejection $\mathcal{R}$ of the first cut could be measured. The background was estimated as $N/(\mathcal{R}-1)$. We ensured unbiased background estimates by dividing

the data into one-third and two-third samples selected uniformly from the entire data set. Selection criteria were determined with the one-third sample and background estimated from the two-third sample. In contrast to the analysis of the pnn1 region, some backgrounds do not have sufficiently distinct characteristics to permit isolation by cut inversion of a pure background sample and permit a measurement of $\mathcal{R}$ with the data. For these backgrounds, we resorted to simulated data to estimate $\mathcal{R}$.

The largest background was due to $K_{\pi 2}$ decays in which the π^+ inelastically scatters in the TG, losing energy and obscuring the directional correlation with the photons from the π^0 decay that would otherwise be detected in the barrel. The two cuts that suppressed this background were identification of π^+ scattering and detection of the photons from π^0 decay. The latter photon veto (PV) ability was improved in E949 with respect to E787 primarily due to the AD and augmentation of the BV by 2.3 r.l. Pion scattering was identified by kinks in the pattern of TG fibers attributed to the outgoing pion, tracks that did not point back to the fiber containing the K^+ decay, energy deposits inconsistent with an outgoing pion or energy deposited in fibers traversed by the kaon at the time of the outgoing pion. The "CCD-PUL" cut identified the latter signature by performing a least-squares fit to the CCD samples to identify the pulses due to activity coincident with the kaon and pion. The uncertainty in the $K_{\pi 2}$ TG-scatter background has comparable statistical and systematic contributions (Table 1). The systematic uncertainty was determined by the range of PV rejection values measured

on samples of $K_{\pi 2}$ scatter events selected by different scattering signatures in the TG or in different kinematic regions. There was also a much smaller background from $K_{\pi 2}$ due to scattering in the RS that was identified by the pattern of RS counters and the energy deposited by the track.

Additional backgrounds included $\mathrm{K}^+ \to \pi^+\pi^0\gamma$ ($K_{\pi 2\gamma}$), $\mathrm{K}^+ \to \pi^+\pi^- e^+\nu$ (K_{e4}), $\mathrm{K}^+\mu^+\nu(\gamma)$ and $\mathrm{K}^+ \to \pi^0\mu^+\nu$ (muon), scattered beam pions (beam) and $\mathrm{K}^0_{\mathrm{L}} \to \pi^+\ell^-\bar{\nu}$ where $\ell^+ = e^+$ or μ^+ resulting from K^+ charge-exchange (CEX) reactions. Simulated data were used to estimate the rejection $\mathcal{R}$ of the cuts that suppress K_{e4}, $K_{\pi 2\gamma}$ and CEX backgrounds. These backgrounds could not be distinguished from the larger $K_{\pi 2}$-scatter background based solely on the π^+ track. The K_{e4} process forms a background when the π^- and e^+ interact in the TG without leaving a detectable trace. Positron interactions are well-modelled in our EGS-based simulation [9] and we used the π^- energy deposition spectrum in scintillator measured previously in E787 [10] to model π^- absorption. We assessed the systematic uncertainty in the K_{e4} background by varying the threshold of cuts on the energy deposited both in the kaon fibers at pion time and in non-kaon and non-pion fibers. The kinematics cuts (KIN) defining the entire signal region were $140 < P < 199$ MeV/c, $60 < E < 100.5$ MeV and $12 < R < 28$ cm. We defined a smaller region $165 < P < 197$ MeV/c, $72 < E < 100$ MeV and $17 < R < 28$ cm where the lower and upper limits were chosen to suppress the K_{e4} background that peaks near 160 MeV/c and the tail of the $K_{\pi 2}$ peak, respectively.

Measurement of the K^+ charge-exchange reaction was used as input to

simulate CEX events [4]. The requirement on the delayed coincidence (DC) between the reconstructed kaon and pion candidates provides suppression of CEX background as the emitted π^+ was required to be within the fiducial region of the TG. The systematic uncertainty was assessed with the same methodology as the K_{e4} background.

The rejection of the $K_{\pi 2\gamma}$ background of the kinematic cuts was calculated using a combination of simulated $K_{\pi 2}$ and $K_{\pi 2\gamma}$ events and $K_{\pi 2}$ data events. The additional PV rejection due to the radiative photon was calculated from the photon distribution in simulated events and the rejection power of single photons as a function of angle and energy evaluated with $K_{\pi 2}$ data [11].

The remaining muon and beam backgrounds were estimated entirely from data and were very small (Table 1). As previous analyses had shown the muon background to be small [5] [6], the TD-based requirements on $\pi^+ \to \mu^+ \to e^+$ identification were loosened to gain acceptance.

The signal region was divided into 9 cells using standard (s) and more restrictive (r) versions of the KIN, TD, DC and PV cuts. The signal region was first divided into two regions defined by $\mathrm{KIN}_s \cdot \overline{\mathrm{KIN}}_r \cdot \mathrm{TD}_s \cdot \mathrm{DC}_s \cdot \mathrm{PV}_s$ and $\mathrm{KIN}_r \cdot \mathrm{TD}_s \cdot \mathrm{DC}_s \cdot \mathrm{PV}_s$. The former region was defined as 1 cell and the latter region was further subdivided into 8 additional cells using the permutations of the TD, DC and PV cuts. The background and acceptance of the best cell, defined as $\mathrm{KIN}_r \cdot \mathrm{TD}_r \cdot \mathrm{DC}_r \cdot \mathrm{PV}_r$, is given in Table 1.

The reliability of the background estimates was checked by loosening the PV and CCDPUL cuts to define three regions just outside the signal region.

Two of the regions, PV_1 and $CCDPUL_1$, were immediately adjacent to the signal region whilst a third region PV_2 was defined by further loosening of the PV cut. The number of expected and observed events and the probability of the observation are given in Table 2. The 5.1% probability for the regions nearest the signal region may have indicated that the background was over-estimated. Given the inability to cleanly isolate each background component by cut inversion, some contamination is possible and would generally inflate the background estimates. Re-evaluation of the probabilities at the lower limit of the systematic uncertainties gave 13.0% for the two closest regions and demonstrated that the assigned systematic uncertainties were reasonable.

After completion of the background studies, the signal region was examined and three candidates were found. The energy *vs* range for the observed candidates is shown in Figure 1 along with the results of previous E787 [3] and E949 [6] analyses. From the observed events, $\mathcal{B}(\mathrm{K}^+ \to \pi^+\nu\bar{\nu}) = (7.89^{+9.26}_{-5.10}) \times 10^{-10}$ was calculated using the likelihood method [8] taking into account the uncertainties in the background and acceptance measurements. When combined with the results of previous E787 [3] and E949 [6] analyses, $\mathcal{B}(\mathrm{K}^+ \to \pi^+\nu\bar{\nu}) = (1.73^{+1.15}_{-1.05}) \times 10^{-10}$ or $< 3.35 \times 10^{-10}$ at 90% CL. This result is consistent with the SM prediction. Assuming $\mathcal{B}(\mathrm{K}^+ \to \pi^+\nu\bar{\nu}) = 1.73 \times 10^{-10}$, the signal-to-background (S/B) ratios for the three candidates are 0.20, 0.42 and 0.48, which can be compared with the S/B = 0.20 for the previous pnn2 candidate [5] and S/B = 59, 8.2 and 1.1 for the pnn1 candidates [3]. As an indication of the improvements in the analysis, a candidate

Bkgd comp.	Cut and additional rejection or acceptance loss KIN	TD	DC	PV	REC	Entire region	Best cell
$K_{\pi 2}$ TG	1.63			2.75	$\surd$	$0.619 \pm 0.150^{+0.067}_{-0.100}$	$0.102 \pm 0.024^{+0.011}_{-0.017}$
$K_{\pi 2}$ RS	1.63			2.75	$\surd$	$0.030 \pm 0.005 \pm 0.004$	$0.005 \pm 0.001 \pm 0.001$
$K_{\pi 2\gamma}$	1.20			$\surd$		$0.076 \pm 0.007 \pm 0.006$	$0.017 \pm 0.002 \pm 0.001$
K_{e4}	2.70			$\surd$		$0.176 \pm 0.072^{+0.233}_{-0.124}$	$0.025 \pm 0.010^{+0.033}_{-0.018}$
CEX			6.7	$\surd$		$0.013 \pm 0.013^{+0.010}_{-0.003}$	$0.001 \pm 0.001^{+0.001}_{-0.000}$
Muon		3.08			$\surd$	0.011 ± 0.011	0.001 ± 0.001
Beam			1.0	$\surd$		0.001 ± 0.001	< 0.001
Total background						$0.927 \pm 0.168^{+0.320}_{-0.237}$	$0.152 \pm 0.027^{+0.047}_{-0.036}$
Acc.	0.812	0.812	0.911	0.522	NA		

Table 1: Summary of the applicable cuts, additional rejection or acceptance loss, contributions to the entire signal region and best cell for each background component. The middle columns indicate the additional rejection for each component from the tightening of the kinematic (KIN), TD, delayed coincidence (DC), photon veto (PV) and reconstruction (REC) cuts. A $\surd$ indicates that the cut was inverted to determine the background. The bottom row gives the relative acceptance loss associated with tightening each cut to divide the signal region into 9 cells. The acceptance of the entire region and best cell was $(1.366 \pm 0.016 \pm 0.052) \times 10^{-3}$ and $(0.436 \pm 0.007^{+0.015}_{-0.019}) \times 10^{-3}$, respectively.

in the best cell (Table 1) would have had S/B=0.84. The probability that the three observed candidates are due to background only, given the estimated background in each cell, is 0.037. The probability that all $K^+ \to \pi^+ \nu\bar{\nu}$ candidates [3] [6] are due to background is 0.001.

Thanks to the usual agencies for their support and the fantastic operation of the AGS.

Region	$N_{\rm exp}$	$N_{\rm obs}$	$\mathcal{P}(\leq N_{\rm obs}; N_{\rm exp})$	Combined
CCD_1	$0.79 \pm 0.35^{+0.30}_{-0.37}$	0	0.452 (0.652)	NA
PV_1	$9.09 \pm 0.65^{+1.38}_{-1.15}$	3	0.020 (0.044)	0.051 (0.130)
PV_2	$32.4 \pm 1.9^{+12.2}_{-7.9}$	34	0.613 (0.973)	0.140 (0.390)

Table 2: Comparison of the expected $N_{\rm exp}$ and observed $N_{\rm obs}$ number of events in three regions CCD_1, PV_1 and PV_2 near the signal region. The central value of $N_{\rm exp}$ is given along with the statistical and systematic uncertainties. $\mathcal{P}(\leq N_{\rm obs}; N_{\rm exp})$ is the probability of observing $N_{\rm obs}$ events or fewer when $N_{\rm exp}$ events are expected. The rightmost column "Combined" gives the probability of the combined observation in that region and the region(s) of the preceding row(s). The numbers in parentheses are the probabilities re-evaluted when $N_{\rm exp}$ is reduced by the systematic uncertainty.

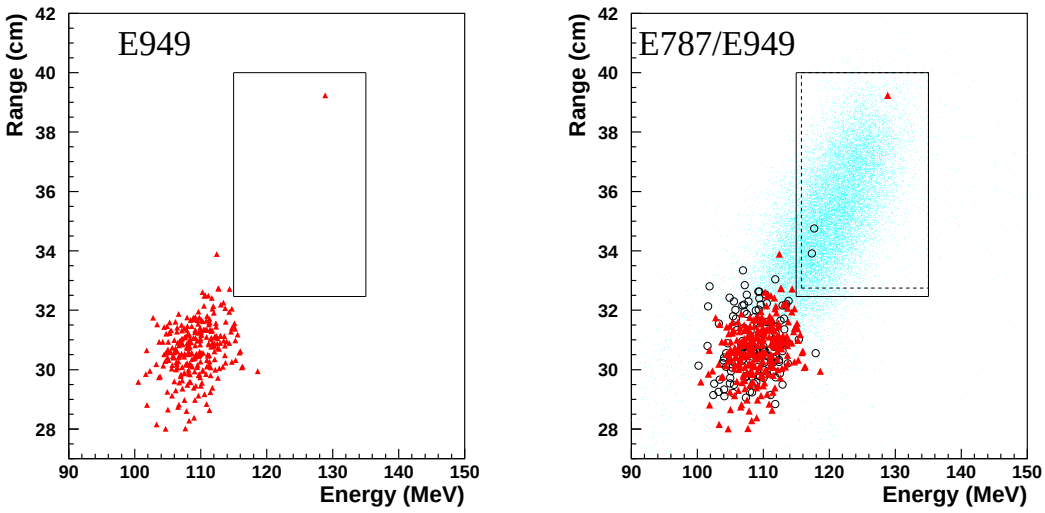

Figure 1: Energy *vs* range plots.**THIS IS A PLACEHOLDER ONLY. Actual figures will show R vs E(or P) of E949 pnn2 candidates and R vs E(or P) of all candidates.**

References

[1] A. J. Buras, F. Schwab and S. Uhlig, arXiv:hep-ph/0405132.

[2] J. Brod and M. Gorbahn, arXiv:0805.4119 [hep-ph]. The uncertainty in the prediction is dominated by the uncertainty in the elements of the CKM matrix.

[3] V.V. Anisimovsky *et al.*, Phys. Rev. Lett. **93**, 031801 (2004)

[4] S. Adler *et al.*, Phys. Rev. D**77**, 052003 (2008).

[5] S. Adler *et al.*, Phys. Lett. B**537**, 211 (2002).

[6] S. Adler *et al.*, Phys. Rev. D**70**, 037102 (2004).

[7] E.W. Blackmore *et al.*, Nucl. Instrum. Methods Phys. Res. A **404**, 295 (1998).

[8] T. Junk, Nucl. Instrum. Methods Phys. Res., Sect. A **434**, 435 (1999).

[9] W. R. Nelson *et al.*, SLAC Report No. SLAC 265, 1985.

[10] M. Ardebili, PhD Thesis, Princeton University,1995.

[11] K. Mizouchi, PhD Thesis, Kyoto University, 2006.